Molecular Biology of the Cell
Vol. 9, 1741–1756, July 1998

The Yeast Dynactin Complex Is Involved in Partitioning the Mitotic Spindle between Mother and Daughter Cells during Anaphase B

Jason A. Kahana,* Gabriel Schlenstedt,* Darren M. Evanchuk,* John R. Geiser,† M. Andrew Hoyt,† and Pamela A. Silver*‡

*Department of Cancer Biology, Dana-Farber Cancer Institute, and Department of Biological Chemistry and Molecular Pharmacology, Harvard Medical School, Boston, Massachusetts 02115; and †Department of Biology, The Johns Hopkins University, Baltimore, Maryland 21218

Submitted December 16, 1997; Accepted April 10, 1998
Monitoring Editor: J. Richard McIntosh

Although vertebrate cytoplasmic dynein can move to the minus ends of microtubules in vitro, its ability to translocate purified vesicles on microtubules depends on the presence of an accessory complex known as dynactin. We have cloned and characterized a novel gene, *NIP100*, which encodes the yeast homologue of the vertebrate dynactin complex protein p150^{glued}. Like strains lacking the cytoplasmic dynein heavy chain Dyn1p or the centractin homologue Act5p, *nip100*Δ strains are viable but undergo a significant number of failed mitoses in which the mitotic spindle does not properly partition into the daughter cell. Analysis of spindle dynamics by time-lapse digital microscopy indicates that the precise role of Nip100p during anaphase is to promote the translocation of the partially elongated mitotic spindle through the bud neck. Consistent with the presence of a true dynactin complex in yeast, Nip100p exists in a stable complex with Act5p as well as Jnm1p, another protein required for proper spindle partitioning during anaphase. Moreover, genetic depletion experiments indicate that the binding of Nip100p to Act5p is dependent on the presence of Jnm1p. Finally, we find that a fusion of Nip100p to the green fluorescent protein localizes to the spindle poles throughout the cell cycle. Taken together, these results suggest that the yeast dynactin complex and cytoplasmic dynein together define a physiological pathway that is responsible for spindle translocation late in anaphase.

INTRODUCTION

One of the main challenges to cells during mitosis is the partitioning of duplicated DNA between dividing cells during anaphase. The early stage of anaphase (termed anaphase A) involves the movement of sister chromatids from the metaphase plate to the spindle poles. During the latter stage known as anaphase B, the mitotic spindle elongates such that the chromosome-associated poles move to opposite ends of the dividing cell. Once the partitioning of genetic material has occurred, the single cell can cleave into two daughter cells, each of which should contain a complete set of chromosomes.

In the budding yeast *Saccharomyces cerevisiae*, anaphase B is particularly complex because the mitotic spindle must be passed through a small (<2-μm-diameter) bud neck rather than simply being pushed to opposite ends of a symmetrically dividing cell. Mutant yeast strains that fail to properly complete anaphase B are characterized by the accumulation of anucleate daughter and binucleate mother cells during vegetative growth. This mitotic defect has been shown to be caused by an inability of the elongating mitotic spindle to enter the daughter cell. As such, a number of factors have been implicated as being responsible for spindle partitioning during anaphase B. These in-

‡ Corresponding author. E-mail address: pamela_silver@dfci.harvard.edu.

clude, most notably, cytoskeletal components such as astral microtubules and actin (Palmer *et al.*, 1992) as well as the microtubule-based motor enzyme cytoplasmic dynein (Eshel *et al.*, 1993; Li *et al.*, 1993).

Purified vertebrate cytoplasmic dynein is capable of binding to microtubules and translocating to their minus ends. However, the transport of purified vesicles to the minus ends of microtubules by highly purified dynein requires additional soluble factors (Paschal and Vallee, 1987; Schroer *et al.*, 1988). A 20S complex termed dynactin was purified from chick brain extracts based on its ability to stimulate dynein-dependent vesicle transport to the minus ends of microtubules (Gill *et al.*, 1991; Schroer and Sheetz, 1991). Included in this complex are conventional actin (Schafer *et al.*, 1994), the actin-related protein Arp1/Centractin (Lees-Miller *et al.*, 1992; Paschal *et al.*, 1993), the α and β subunits of the actin-capping protein (Schafer *et al.*, 1994), the homologue of the *Drosophila* Glued protein (p150^{glued}; Gill *et al.*, 1991), as well as polypeptides of 62, 50 (p50), 27, and 24 kDa (Schroer and Sheetz, 1991). Furthermore, the complex is highly conserved throughout metazoan evolution and has been described not only in chicken but also in bovine brain and *Drosophila* extracts (Paschal *et al.*, 1993; McGrail *et al.*, 1995; Waterman-Storer and Holzbaur, 1996).

Based on the in vitro requirement for dynactin in vesicle transport, it is plausible that the in vivo function of cytoplasmic dynein is dependent on the activity of the dynactin complex. This hypothesis is supported by the findings that yeast strains harboring deletions of the *ACT5* gene (which encodes the yeast homologue of Arp1p) have anaphase defects indistinguishable from strains lacking the cytoplasmic dynein heavy chain Dyn1p. Like *dyn1*Δ strains, *act5*Δ strains accumulate binucleate mother and anucleate daughter cells as a result of a diminished ability to pass their anaphase mitotic spindles through the bud neck (Clark and Meyer, 1994; McMillan and Tatchell, 1994; Muhua *et al.*, 1994).

Although the terminal phenotypes of strains lacking dynactin homologues are well defined, it is not yet clear how the complex assembles and functions to ensure proper polarized cell division in yeast. In this study, we identify and characterize the *NIP100* gene, which encodes the yeast homologue of the dynactin complex protein p150^{glued}. Like *act5*Δ and *dyn1*Δ strains, *nip100*Δ strains are viable but undergo failed mitoses in which chromatid separation and mitotic spindle elongation occur completely within the mother cell. Moreover, the precise mitotic defect of *nip100*Δ cells is a failure to translocate elongated spindles into the bud during anaphase. Furthermore, we demonstrate that there exists a stable physiological interaction between Nip100p and Act5p that is dependent on the presence of Jnm1p, another factor previously shown to be required for accurate spindle partitioning (McMillan and Tatchell, 1994). Finally, we show that this complex is localized to the spindle poles throughout the cell cycle. These results suggest a model by which the dynactin complex cooperates with dynein to effect spindle translocation during late anaphase.

MATERIALS AND METHODS

Standard Techniques

Media preparation and genetic techniques have been previously described (Sherman *et al.*, 1986). Yeast transformations were performed using the lithium acetate procedure (Gietz and Schiestl, 1991). Standard molecular biological techniques were performed as described (Sambrook *et al.*, 1989). All restriction and DNA-modifying enzymes were purchased from New England Biolabs (Beverly, MA). All PCR amplifications were performed using Vent DNA polymerase to minimize errors. Purified Tween 20 detergent was purchased from Bio-Rad (Hercules, CA). All other reagents were purchased from Sigma Chemical (St. Louis, MO).

Plasmid Construction

The two-hybrid screen using Nup1p as bait has been previously described (Osborne *et al.*, 1994).

pPS374. This plasmid is the original two-hybrid interactor encompassing a fusion of the *GAL4* activation domain to a 4.6-kb genomic *Sau*3A fragment spanning a region from nucleotide 568 of the *NIP100* open reading frame to 2610 nucleotides 3′ of the stop codon.

pPS375. This is a 4.2-kb *Kpn*I–*Hin*DIII fragment encompassing 1.2 kb of 5′ promoter sequence, the 2607-bp open reading frame, and 410 bp of the 3′ untranslated region of the *NIP100* genomic locus in pBluescript (Stratagene, La Jolla, CA). Recovery of the 5′ end of *NIP100* was performed as previously described (Roeder and Fink, 1980; Osborne *et al.*, 1994).

pJK48. This is a 2μ (multicopy) vector encoding the *NIP100* ORF with the 200 bp 5′ untranslated promoter region fused in-frame to the [S65T; V163A] mutant of the green fluorescent protein (sGFP[1]; Kahana and Silver, 1996). The 2.8-kb fragment was PCR-amplified from the pPS375 template using the *Bam*HI- and *Sal*I-linked primers: 5′-CggatccGCATATATGTTGAAAAGTCAC-3′ and 5′-GTGGgtcgacCTTTGTAATATGTAACAAC-3′. The PCR product was cut with *Bam*HI and *Sal*I and ligated into pJK26-19-1, a 2μ, LEU2-containing vector for expression of NUF2-GFP, which had been cut with *Bam*HI and *Xho*I.

pJK52. The 2.3-kb *Bam*HI–*Hin*DIII fragment encoding the *NUF2* promoter and ORF ligated to GFP was excised from pJK26-19-1. The *NUF2* 3′ untranslated region (UTR) sequence was amplified from the genomic clone pPS511 using the T3 sequencing primer and the *Hin*DIII-linked primer: 5′-GGCaagcttCGGTATACTTATTTTTAC-3′. The resulting PCR product was digested with *Hin*DIII and *Kpn*I. Finally, the two fragments were ligated into the TRP1-containing centromeric (CEN) plasmid pRS314 (Sikorski and Hieter, 1989) cut with *Bam*HI and *Kpn*I.

pJK67. This is a vector for replacement of the endogenous NUF2 gene with the *NUF2*-GFP gene. A 3.3-kb *Nhe*I–*Kpn*I fragment containing the partial *NUF2-GFP* ORF and the entire 3′ UTR was excised from pJK52 and ligated into the integrating vector pRS306 (Sikorski and Hieter, 1989), which had been cut with *Xba*I and *Kpn*I.

pJK75. A 3.6-kb fragment encompassing the entire *NIP100* gene was amplified by PCR using pPS375 as template and the following

[1] Abbreviations used: CEN, centromeric; GFP, green fluorescent protein; HA, hemagglutinin; IgG, immunoglobulin G; sGFP, mutant [S65T; V163A] GFP; SPB, spindle pole body; UTR, untranslated region.

*Bam*HI and *Sal*I-linked primers: 5′-GGggatccACTGGAACAGTCTTTGTGGG-3′ and 5′-CATGgtcgacTTGGACACTTCCCTCTTTTCATG-3′. The resulting PCR product was cut with *Bam*HI and *Sal*I and ligated into a similarly cut CEN/TRP1 plasmid, pRS314 (Sikorski and Hieter, 1989).

pJK76. The same 3.6 kb fragment was ligated into the CEN/URA3 plasmid pRS316 (Sikorski and Hieter, 1989) cut with *Bam*HI and *Sal*I.

pJK93. This is a vector for the expression of protein A (4Z)-tagged Nuf2p. The *Xho*I–*Hin*DIII fragment encompassing the sGFP sequence was excised from pJK50 (a URA3 version of pJK52) and replaced with an *Xho*I–*Hin*DIII fragment encoding four tandem repeats of the immunoglobulin G (IgG) binding domain of protein A and a 6x His tag (Grandi *et al.*, 1993).

pJK90. This is a vector for the expression of 4Z-tagged Nip100p. A fragment encoding a 692-bp upstream promoter and full-length ORF sequence of *NIP100* was amplified using pJK75 as template and the following *Bam*HI- and *Sal*I-linked primers: 5′-GGggatccACTGGAACAGTCTTTGTGGG-3′ and 5′-GTGGgtcgacCTTTGTAATATGTAACAAC-3′. The resulting PCR product was digested with *Bam*HI and *Sal*I and ligated into pJK93, which had been cut with *Bam*HI and *Xho*I.

pJK94. This is a vector for the expression of the 4Z tag from the *NIP100* promoter. A fragment encoding the *NIP100* promoter and an in-frame start codon was amplified using pJK75 as a template and the following *Bam*HI and *Xho*I-linked primers: 5′-GGggatccACTGGAACAGTCTTTGTGGG-3′ and 5′-TAGctcgagCATTGCGCATTTGTCCAAGGCTG-3′. The resulting PCR product was cut with *Bam*HI and *Xho*I and ligated into pJK93, which had been cut with *Bam*HI and *Xho*I.

pJK108. This is a vector for the expression of 4Z-tagged Pac11p. A fragment encoding the *PAC11* promoter and ORF was PCR amplified using genomic DNA as template and the following *Bam*HI- and *Xho*I-linked primers: 5′-GggatccTCGACAGCAGTAGTTTCC-3′ and 5′-GGctcgagCGGAGATAACAGTGGCCGTG-3′. The resulting PCR product was cut with *Bam*HI and *Xho*I and ligated into pJK93, which had been cut with *Bam*HI and *Xho*I.

pJK132. This is a vector for the expression of Nip100-sGFP from the inducible *GAL1–10* promoter. A DNA fragment encompassing the entire *NIP100* ORF was PCR amplified using the following *Bam*HI- and *Sal*I-linked primers: 5′-GCggatccATGCGCAATGCAGGTGTTC-3′ and 5′-GTGGgtcgacCTTTGTAATATGTAACAAC-3′. The resulting PCR product was cut with *Bam*HI and *Sal*I and ligated with an *Xho*I–*Hin*DIII fragment encompassing the sGFP coding sequence into pPS311 (A CEN LEU2 GAL1–10 vector), which had been cut with *Bam*HI and *Hin*DIII.

pJK138. This is a vector for the replacement of the *NIP100* ORF with the *NIP100-3xHA* fusion. The PCR product used for pJK132 was cut with *Xba*I and *Sal*I and ligated into pJK137, a yeast integrating URA3 vector, which has three tandem repeats of the coding sequence for the hemagglutinin (HA) tag (YPYDVPDYA) as well as the *NUF2* 3′ UTR.

pJG220. This is a vector for 3xHA tagging of the genomic copy of *DYN1*. A 293-bp fragment immediately 5′ of the *DYN1* stop codon was PCR-amplified with *Sac*II restriction site ends using genomic DNA as template. This fragment was cloned in-frame into the *Sac*II site of pWS9936, a 3xHA-containing vector (a gift of B. Futcher, Cold Spring Harbor Laboratories, Cold Spring Harbor, NY). This creates a plasmid (pJG215) that has 293 bp before the stop codon of *DYN1* in-frame with the coding sequence of the first 3xHA, resulting in the following construct: *DYN1*-3xHA-*URA3*-3xHA. A 187-bp fragment containing the stop codon and sequences 3′ of the *DYN1* coding region was PCR amplified with *Xho*I–*Kpn*I ends using genomic DNA as template. This fragment was cloned, in-frame, into the *Xho*I–*Kpn*I sites of pJG215. This creates a plasmid that has 187 bp of *DYN1* terminator immediately following the 3xHA. The stop codon of *DYN1* is in-frame with the last amino acid of the 3xHA tag. This results in the following construct: *DYN1*-3xHA-*URA3*-3xHA-(stop)-*DYN1*-3′ UTR.

Strain Construction

A complete disruption of the *NIP100* gene was made using the PCR-based method of Baudin *et al.* (1993) using the following primers: 5′-ACAGTTGTAAGGTGCTTTCTTTTTACTCTAACCTCCACACTGAGATTGTTGGCCTCCTCTAGTACACTC-3′ and 5′-CTTGCGCTTTAAATACGAAATGTAAGAATGATCTCTTTCATGCCAGAGTTGCGCGCCTCGTTCAGAATG-3′. The resulting PCR product (*HIS3* with 50 bp of *NIP100* sequence on each end) was transformed into diploid strain PSY613 and plated on media lacking histidine. His^+ colonies were isolated and tested for correct integration of *HIS3* at the *NIP100* locus by genomic PCR and Southern blotting. Proper integration of the PCR fragment at the *NIP100* locus results in ablation of a region spanning 130 bp 5′ of the *NIP100* ATG to the end of the ORF. Because the gene is not essential, we used the same technique to disrupt *NIP100* in the haploid S288c-based strains FY86 and JKY196.

*act5*Δ*::HIS3* and *jnm1*Δ*1::LEU2* strains were made as described by Muhua *et al.* (1994) and McMillan and Tatchell (1994), respectively.

Nuf2-sGFP–expressing strains were constructed as follows. Plasmid pJK67 was linearized by digestion with *Bst*EII and transformed into haploid strains FY86 (wild type) and JKY77 (*nip100*Δ). Ura^+ colonies were recovered and tested for replacement of the endogenous *NUF2* gene with *NUF2-sGFP* by immunoblot analysis of whole-cell extracts using the α-Nuf2p monoclonal antibody 5B7-13 (Osborne *et al.*, 1994). Both wild-type and *nip100*Δ strains expressing Nuf2-sGFP (JKY85 and JKY86) grow at rates indistinguishable from isogenic strains expressing wild-type Nuf2p.

The Nip100-3xHA–expressing strains (JKY277 and JKY278) were constructed by linearization of pJK138 with *Cla*I, transformation into haploid strains, and isolation of Ura^+ colonies. For testing whether Nip100-3xHA is functional, linearized pJK138 was transformed into JKY50, a diploid *cin8*Δ*::LEU2/CIN8* strain. The transformed diploid was tested for proper replacement of *Nip100* with *Nip100-3xHA* and sporulated. Approximately 25% of the viable spores were Ura^+, Leu^+, signifying that the fusion protein is functional. Moreover, we observe <2% binucleate cells in cultures of strains expressing Nip100-3xHA in place of Nip100p.

The HA-tagged dynein heavy chain–expressing strain MAY3613 was constructed by the method of Schneider *et al.* (1995). The insert of pJG220 was liberated with BssHII and transformed into wild-type strain MAY591. Ura^+ colonies were isolated and grown in YEPD medium. Cells were then plated to 5′-fluoroorotic acid to select for "looping out" of the URA3 gene by mitotic recombination. Looping out of URA3 results in a 3xHA-labeled DYN1 (and no extra DNA). Correct in-frame integration of the HA tag at the 3′ end of *DYN1* was confirmed by PCR amplification and sequencing of the genomic allele. Strains harboring the tagged *DYN1-3xHA* allele do not exhibit the anaphase defect of *dyn1*Δ strains, as assayed by DAPI staining of chromatin. Furthermore, *cin8*Δ*; DYN1::3xHA* strains are viable.

Microscopy Techniques

Visualization of spindle pole bodies (SPBs) in live cells is based on the technique of Kahana *et al.* (1995). Microscope growth chambers were prepared as follows. Microscope slides were coated with 1 ml of molten SC-ura/1% agarose. Next, a second slide was placed on top, and the "sandwich" was allowed to cool to room temperature. The top slide was removed, and 3 μl of cells from a logarithmic overnight culture were placed in the center of the solidified medium. A 22 × 22-mm number 1½ cover slide was placed over the cells, and the remaining solid medium was cut away with a razor blade. Finally, the coverslip was sealed with molten VALAP (1:1:1 petroleum jelly:lanolin:paraffin) wax. During observations, the slides were maintained at 25°C using a thermostat-controlled heated microscope stage insert (Micro Video, Avon, MA).

Observations were taken on a Nikon Diaphot 300 inverted microscope equipped with a 100× 1.4 numerical aperture Plan-Apo objective lens, a 100 W Hg epifluorescence illuminator, and GFP filter set 41018 (Chroma Technology, Brattleboro, VT). Digital images

were obtained using a CH250/KAF1400 cooled charge-coupled device camera (Photometrics, Phoenix, AZ), which was controlled by Metamorph 2.5 software (Universal Imaging, West Chester, PA). Cells were observed using 50-ms exposures taken every 10 s with manually controlled motorized focusing. Fluorescence illumination was controlled by a Uniblitz shutter (Vincent Associates, Rochester, NY), which was synchronized with the camera shutter.

The distance between SPBs was measured using the "measure distance" feature of the Metamorph software calibrated to a 10 μm stage micrometer. Total magnification to the charge-coupled device array resulted in 14.67 camera pixels per micrometer. Rate measurements were taken only when both SPBs were in focus. Rates were determined by linear regression and curve fitting using Cricket Graph software (Computer Associates, Islandia, NY).

Static observations of SPB morphology was performed as follows. Strains JKY85 and JKY86 were grown overnight in SC-ura medium at 30°C to OD_{600} = 0.7. The cultures were then diluted 1:50 in fresh media and grown at 12, 25, 30, and 36°C. Cultures were directly observed by fluorescence microscopy when they had grown to a density of OD_{600} = 0.6–0.7.

Immunofluorescence detection of Nip100-sGFP and microtubules was performed as follows. Strain JKY77 (*nip100*Δ) was transformed with plasmid pJK48 (2μ Nip100-sGFP LEU2). Transformants were grown to OD_{600} = 0.7 in SC-Leu medium, fixed for 30 min at 25°C in 3.7% formaldehyde, and processed for immunofluorescence as previously described (Pringle *et al.*, 1991). A polyclonal rabbit α-GFP antibody (Clontech, Palo Alto, CA) was used at a 1:1000 dilution, and the rat monoclonal α-tubulin antibody YOL1/34 (Serotec) was used at a 1:25 dilution. FITC-conjugated α-rabbit IgG and Texas Red-conjugated α-rat IgG secondary antibodies (Jackson Immunochemicals, West Grove, PA) were used at 1:500 dilutions. Chromatin was visualized by washing cells with 1 μg/ml DAPI in PBS.

For "pulse–chase" visualization of Nip100-sGFP, strain JKY184 (*nip100*Δ*::HIS3*) carrying pJK132 was grown overnight in SC-Leu media containing 2% raffinose as the sole carbon source at 30°C. Galactose was added to a final concentration of 2%, and the cells were grown 30 min at 30°C. The cells were then collected by centrifugation, resuspended in SC-Leu containing 2% glucose, and grown for 3 h at 30°C. Live cells were observed by placing 3 μl of the culture directly on a microscope slide and visualized using fluorescence and differential interference contrast microscopy. Approximately 10% of fluorescent cells had three to eight dots of staining. Immunofluorescence with anti-tubulin antibodies indicated that the dots are associated with multiple SPBs (which likely arise because the cells are phenotypically $Nip100^-$ in the presence of raffinose and glucose).

Isolation of Tagged Nip100p from Cell Extracts

Nip100-3HA–expressing strains JKY277 and JKY278 (*dyn1*Δ) were grown in 50 ml YEPD at 30°C to OD_{600} = 1.0–1.2. Cells were isolated by centrifugation and resuspended in 1 ml GFO buffer (50 mM Tris, pH 8.0, 150 mM NaCl, 2 mM $MgCl_2$, ±0.2% Tween 20) with Complete protease inhibitor mixture (Boehringer Mannheim, Indianapolis, IN) and 500 μl acid-washed glass beads. The cells were lysed in a bead beater (Biospec Products, Bartlesville, OK) by agitation at 5000 rpm three times for 30 s each at 4°C. Approximately 90% of the cells are lysed by this method.

For determination of solubility, lysates made in the presence or absence of detergent were spun 15 min at 13,000 rpm in a microcentrifuge (Eppendorf 5415). The resulting low-speed supernatants were then centrifuged at 55,000 rpm in a Beckman (Fullerton, CA) TLA100.2 rotor (~100,000 × *g*) at 4°C for 30 min. Equal fractions of whole-cell extract, low-speed supernatant, low-speed pellet, high-speed supernatant, and high-speed pellet were resuspended into 1× sample buffer and analyzed by SDS-PAGE and immunoblot using the 12CA5 anti-HA monoclonal antibody (Boehringer Mannheim).

For sucrose density gradient centrifugation, the detergent lysate was directly spun at 55,000 rpm in a TLA100.2 rotor (~100,000 × *g*) at 4°C for 15 min, and 500 μl of the soluble extract were layered atop a 10-ml linear gradient of 7–18% sucrose in GFO buffer containing 0.2% Tween 20. Purified thyroglobulin (19.4S), catalase (11.3S), and yeast alcohol dehydrogenase (7.4S) suspended in 500 μl GFO buffer were used as density standards. Gradients were spun at 34,000 rpm for 17 h at 4°C in an SW41 rotor. Ten ~1-ml fractions were collected, and a portion of each fraction was diluted 1:1 in 2× protein sample buffer. Samples were analyzed by SDS-PAGE and immunoblotting with antibodies against the HA tag, Jnm1p (a gift of M. Company, J. McMillan, and K. Tatchell, Louisiana State University Medical Center, Shreveport, LA), or Act5p (a gift of S. Clark and D. Meyer, University of California, Los Angeles, CA).

Strain MAY3613 was transformed with plasmids pJK90 (encoding Nip100-4Z), pJK93 (Nuf2-4Z), pJK94 (4Z), and pJK108 (Pac11-4Z). The resulting transformants were grown overnight at 30°C in SC-ura medium to a density of OD_{600} = 1.0–1.2. Cells were harvested and lysed in GFO buffer as described above. The lysate was spun at 13,000 rpm in a microcentrifuge at 4°C for 10 min, and the soluble extract was transferred to a clean tube. To this, 50 μl of IgG-Sepharose 6FF beads (Pharmacia, Uppsala, Sweden) were added, and the mixture was incubated with agitation for 5 min at room temperature. The tubes were then centrifuged for 30 s at 5000 rpm in a microcentrifuge, and the supernatant was removed. The beads were then washed four times with 1 ml GFO buffer. A 100-μl aliquot of the supernatant was diluted 1:1 with 2× protein sample buffer, and the bound IgG beads were resuspended in 100 μl 1× protein sample buffer.

Bound proteins were visualized by SDS-PAGE and immunoblotting as follows. Twenty microliters of each sample were run on a 6% (for Dyn1-3xHA) or 10% SDS-polyacrylamide gel, blotted to nitrocellulose, and probed with antibodies against the HA tag, Act5p, or Jnm1p. HRP-conjugated secondary antibodies with minimal cross-reactivity to human IgG (Jackson Immunochemicals) were used to prevent detection of the human IgG heavy and light chains eluted from the affinity matrix. Visualization of blots was performed using the ECL reagent (Amersham, Buckinghamshire, United Kingdom) as directed by the manufacturer.

RESULTS

Nip100 Is the yeast Homologue of the Vertebrate Dynactin Complex protein p150^{glued}

The *NIP100* gene was originally isolated in a two-hybrid screen for proteins that could interact with the nucleoporin Nup1p. In addition to Nip100, the previously reported SPB-associated protein Nuf2p was identified in this screen (Osborne *et al.*, 1994). Because neither Nip100p nor Nuf2p colocalizes with known nuclear pore proteins (see below), it is not clear whether the interaction observed in the two-hybrid screen is physiologically relevant. Recently, the *NIP100* gene has been cloned in a screen for genes that were essential in the absence of the kinesin-like protein-encoding gene *CIN8* (Geiser *et al.*, 1997).

Sequencing of the complete *NIP100* locus reveals a 2604-bp open reading frame, which encodes a protein of predicted molecular mass of 100 kDa. Sequence analysis of the Nip100 protein indicates that it is homologous to the rat dynactin complex protein p150^{glued} and the cytoplasmic vesicle linker protein CLIP-170 (Altschul *et al.*, 1990; Holzbaur *et al.*, 1991; Pierre *et al.*, 1992). In particular, the three proteins are particularly homologous over a conserved N-terminal region, which has been implicated in microtubule

Table 1. Yeast strains used in this study

Strain	Genotype	Source
PSY613	*Mat* **a**/α; *ura3/ura3; leu2/leu2; his3Δ200/his3Δ200; ADE3/ade3; ade2/ADE2; trp1/TRP1; lys2/LYS2*	This study
JKY83	*Mat* **a**/α; *ura3/ura3; leu2/leu2; his3Δ200/his3Δ200; ADE3/ade3; ade2/ADE2; trp1/TRP1; lys2/LYS2; nip100Δ::HIS3/NIP100*	This study
FY86	*Mat α; ura3-52; leu2Δ1; his3Δ200*	Winston *et al*. (1995)
JKY77	*Mat α; ura3-52; leu2Δ1; his3Δ200; nip100Δ::HIS3*	This study
JKY85	*Mat α; ura3-52; leu2Δ1; his3Δ200; nuf2Δ::NUF2-GFP::URA3*	This study
JKY86	*Mat α; ura3-52; leu2Δ1; his3Δ200; nip100Δ::HIS3; nuf2Δ::NUF2-GFP::URA3*	This study
JKY196	*Mat* **a**; *ura3-52; leu2Δ1; his3Δ200; trp1Δ63*	This study
JKY122	*Mat* **a**; *ura3-52; leu2Δ1; his3Δ200; trp1Δ63; act5Δ::HIS3*	This study
JKY184	*Mat* **a**; *ura3-52; leu2Δ1; his3Δ200; trp1Δ63; nip100Δ::HIS3*	This study
JKY231	*Mat* **a**; *ura3-52; leu2Δ1; his3Δ200; trp1Δ63; jnm1Δ1::LEU2*	This study
JKY277	*Mat* **a**; *ura3-52; leu2Δ1; his3Δ200; trp1Δ63; nip100Δ::NIP100-3xHA::URA3*	This study
JKY278	*Mat* **a**; *ura3-52; leu2Δ1; his3Δ200; trp1Δ63; dyn1Δ::HIS3; nip100Δ::NIP100-3xHA::URA3*	This study
MAY591	*Mat α; lys2-801; his3Δ200; leu2-3,112; ura3-52*	This study
MAY3613	*Mat α; lys2-801; his3Δ200; leu2-3,112; ura3-52; DYN1::3xHA*	This study
JKY218	*Mat α; lys2-801; his3Δ200; leu2-3,112; ura3-52; DYN1::3xHA; act5Δ::HIS3*	This study
JKY220	*Mat α; lys2-801; his3Δ200; leu2-3,112; ura3-52; DYN1::3xHA; jnm1Δ1::LEU2*	This study

binding (Figure 1A) (Pierre *et al*., 1992; Waterman-Storer *et al*., 1995).

Although Nip100p has only 13.7% overall sequence similarity to p150^{glued}, their predicted secondary structures are similar. Using the COILS algorithm (Lupas *et al*., 1991), both proteins are predicted to comprise of N- and C-terminal coiled-coil–forming regions separated by a central noncoiled region (Figure 1B). In contrast, CLIP-170 is predicted to have a single coiled-coil–forming region from amino acids 350-1310, comprising ~70% of the protein (Pierre *et al*., 1992, 1994). Because the primary and secondary sequence analyses suggest that Nip100p is indeed the yeast homologue of the vertebrate dynactin complex protein p150^{glued}, a functional analysis of the gene was undertaken.

nip100Δ Strains Are Viable but Defective in Anaphase Spindle Translocation

Using a PCR-based approach, we replaced a single copy of the *NIP00* open reading frame in a wild-type diploid yeast strain with the *HIS3* gene by homologous recombination (Baudin *et al*., 1993). Correct integration of the *HIS3* gene at the *NIP100* locus was confirmed by genomic PCR and Southern blot analyses. The resulting heterozygous *nip100Δ::HIS3/NIP100* strain was sporulated, and 33 of 36 (92%) of the resulting tetrads were four-spored. All 33 of the four-spored tetrads exhibited 2:2 segregation of the *HIS3* locus, indicating that *NIP100* is not an essential gene. Furthermore, *nip100Δ* strains are capable of growth at temperatures ranging from 12 to 36°C. However, even under optimal conditions the growth rate of *nip100Δ* strains is slower than that of wild-type strains; the doubling time at 30°C in YPD medium is 100 min for wild-type and 135 min for *nip100Δ* cells.

Like strains lacking cytoplasmic dynein, Act5p, or the Jnm1 protein (McMillan and Tatchell, 1994), *nip100Δ* strains exhibit "internal mitoses" in which anaphase spindle elongation occurs completely within the mother cell. By using a fusion of the *Aequorea victoria* GFP to the yeast SPB protein Nuf2p (Kahana *et al*., 1995), we were able to determine spindle positioning in vegetatively growing wild-type and *nip100Δ* cells. Cells constitutively expressing Nuf2-GFP were grown to early logarithmic phase at 12, 25, 30, and 36°C and observed with a fluorescence microscope. As shown in Figure 2A, wild-type cells exhibit four typical spindle morphologies: a single SPB at the bud neck in G_1 (type I); a "side-by-side" set of duplicated SPBs typical of early S phase (type II); a short (1- to 2-μm) spindle in late S/early M phase (type III); and an elongated anaphase spindle, which is partitioned between mother and daughter cells (type IV). Although most *nip100Δ* cells exhibit spindle morphologies I–IV, we have observed a number of aberrant morphologies as well: an elongated (4- to 5-μm) spindle that has not entered the daughter cell but remains pointed toward the bud neck (type V); an elongated spindle that is not aligned along the mother–bud axis (type VI); a posttelophase set of SPBs, which remain within the mother cell (type VII); and extra (>2) SPBs in the mother cell (type VIII). Moreover, we note that the aberrant morphologies are more prevalent at low temperature (37% total at 12°C vs. 16% at 30°C). In contrast, we observed only 1% of wild-type cells exhibiting type V morphology and none exhibiting type VI–VIII morphologies at all temperatures tested. Anti-tubulin immunofluorescence and DNA staining with DAPI reveals that *nip100Δ* cells exhibiting type V and VI morphologies have separated masses of DNA, an elongated mitotic

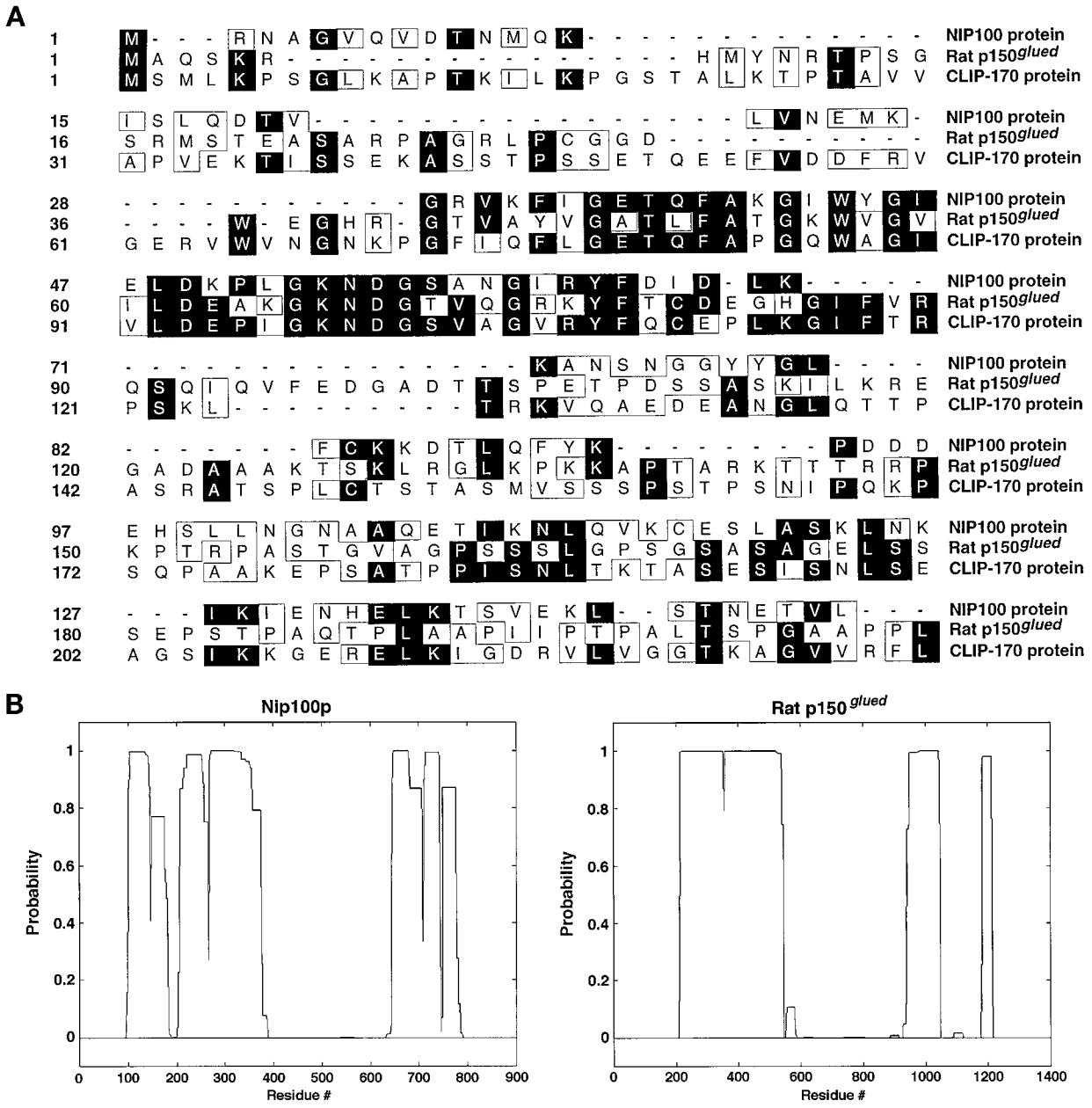

Figure 1. Similarity between Nip100p and p150^{glued}. (A) Sequence alignment of the N-terminal regions of Nip100p and p150^{glued}. Identical residues are shown in inverse; similar residues are boxed. Sequence alignment was performed using the Megalign module from the Lasergene software package (DNAstar, Madison, WI). (B) Predicted coiled-coil structure of Nip100p and rat p150^{glued}. Predictions were performed using the COILS algorithm of Lupas *et al.* (1991) with a window of 28 residues.

spindle, and astral microtubules extending into the bud. Furthermore, the astral microtubules may be extremely long and curve around the daughter cell cortex (Figure 2B). In summary, although *nip100*Δ strains generally exhibit normal microtubule structure and chromatid separation during anaphase, they are deficient in their ability to pass the mitotic spindle into the daughter cell.

In Vivo Analysis of nip100Δ Strains Indicates That Nip100p Is Specifically Required for Spindle Translocation

The binucleate phenotype typical of nip100Δ strains has been associated with loss of function of either dynein (Eshel *et al.*, 1993; Li *et al.*, 1993) or the kinesin-like protein Kip3p (Cottingham and Hoyt, 1997;

A

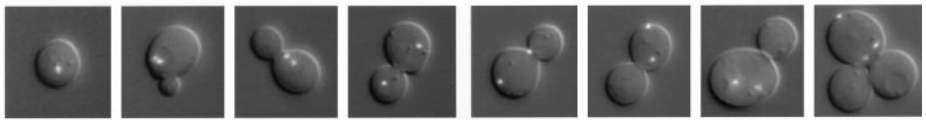

		I	II	III	IV	V	VI	VII	VIII
12°	*NIP100*	48%	22	9	20	1	0	0	0
	nip100Δ	23	20	11	9	3	13	9	12
25°	*NIP100*	35	18	11	34	1	0	0	0
	nip100Δ	26	12	12	26	12	3	2	7
30°	*NIP100*	30	17	12	40	1	0	0	0
	nip100Δ	26	16	10	33	10	2	0	4
37°	*NIP100*	30	25	15	28	1	0	1	0
	nip100Δ	34	16	14	15	3	7	4	7

B

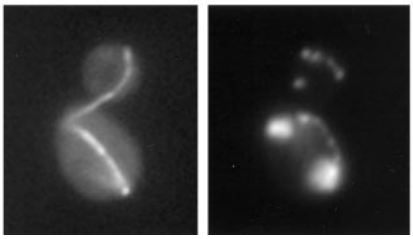

Figure 2. Anaphase defect of *nip100*Δ cells. (A) Spindle morphologies of wild-type and *nip100*Δ strains. Strains JKY85 (wild-type) and JKY86 (*nip100*Δ*::HIS3)* expressing the Nuf2-GFP SPB tag were grown to OD_{600} = 0.6–0.8 and observed on a fluorescence microscope with an FITC filter set. An overlay of Nuf2-GFP with a differential interference contrast image of cells representing each of the typical morphologies is shown along with the percentage of wild-type and *nip100*Δ cells exhibiting each morphology at 12, 25, 30, and 37°C (n > 100 cells for each sample). Morphologies I–IV are wild-type (G_1, S, G_2–M, and M phase, respectively), whereas morphologies V–VIII represent the mutant phenotype of *nip100*Δ cells. (B) Fluorescence micrographs of a typical type V *nip100*Δ cell. Microtubules were visualized by indirect immunofluorescence using a monoclonal antibody against α-tubulin. DNA was visualized with DAPI. Note that, although the spindle has failed to enter the daughter cell, astral microtubules have passed through the bud neck, and sister chromatids have separated.

DeZwaan et al., 1997). Whereas *kip3*Δ cells become binucleate as a result of failure to position the mitotic spindle at the bud neck before mitosis (DeZwaan et al., 1997), *dyn1*Δ cells become binucleate because of their inability to translocate the spindle through the bud neck during anaphase B (Yeh *et al.*, 1995). Although dynactin was originally characterized in vitro as an accessory factor for purified cytoplasmic dynein, it is a possibility that, in vivo, it acts on kinesin-like proteins as well in the positioning step. Hence, to determine the precise mitotic defect that elicits the aberrant morphologies observed in *nip100*Δ cells, we used an in vivo assay to determine spindle dynamics.

Using Nuf2-GFP, we have previously shown that anaphase in wild-type cells comprises four steps. First, the preanaphase B spindle moves to the bud neck and aligns along the mother–bud axis of division. Second, the spindle begins to elongate within the mother cell. Third, the partially elongated spindle translocates, as a unit, through the bud neck such that it is partitioned between mother and daughter cells. Finally, the spindle continues to elongate, but at a rate approximately one-half that of the original rate (Kahana *et al.*, 1995). In vivo analysis reveals that the spindle migration defect observed in *nip100*Δ cells is not due to an inability to align the mitotic spindle at the bud neck. Like wild-type strains, *nip100*Δ strains properly position their short (preanaphase B) spindles at the bud neck before anaphase spindle elongation. Furthermore, the spindles are properly aligned within 20° of the mother–bud axis of division in all wild-type and *nip100*Δ cells observed (Figure 3).

However, whereas wild-type strains typically translocate their partially elongated (~3- to 3.5-μm) spindles through the bud neck within 2–3 min after spindle elongation occurs (n = 13; Figure 3, A, 230–360 s, B, 130–160 s), this stage of anaphase is generally not observed in *nip100*Δ cells. Instead, as with cells lacking cytoplasmic dynein (Yeh *et al.*, 1995), spindle elongation through the bud neck, rather than translocation, is the general means by which *nip100*Δ cells partition the mitotic spindle between the mother and daughter cells. In these cells, the spindle elongates to a length of 4.5–5 μm within the mother until the mother cell's SPB has moved all the way to the distal end of the cell cortex (Figure 3, C and D). Then, the spindle either elongates through the bud neck immediately (Figure 3C), becomes stuck at the bud neck for an extended period and then passes through (Figure 3D), or remains stuck for an extended period and then falls

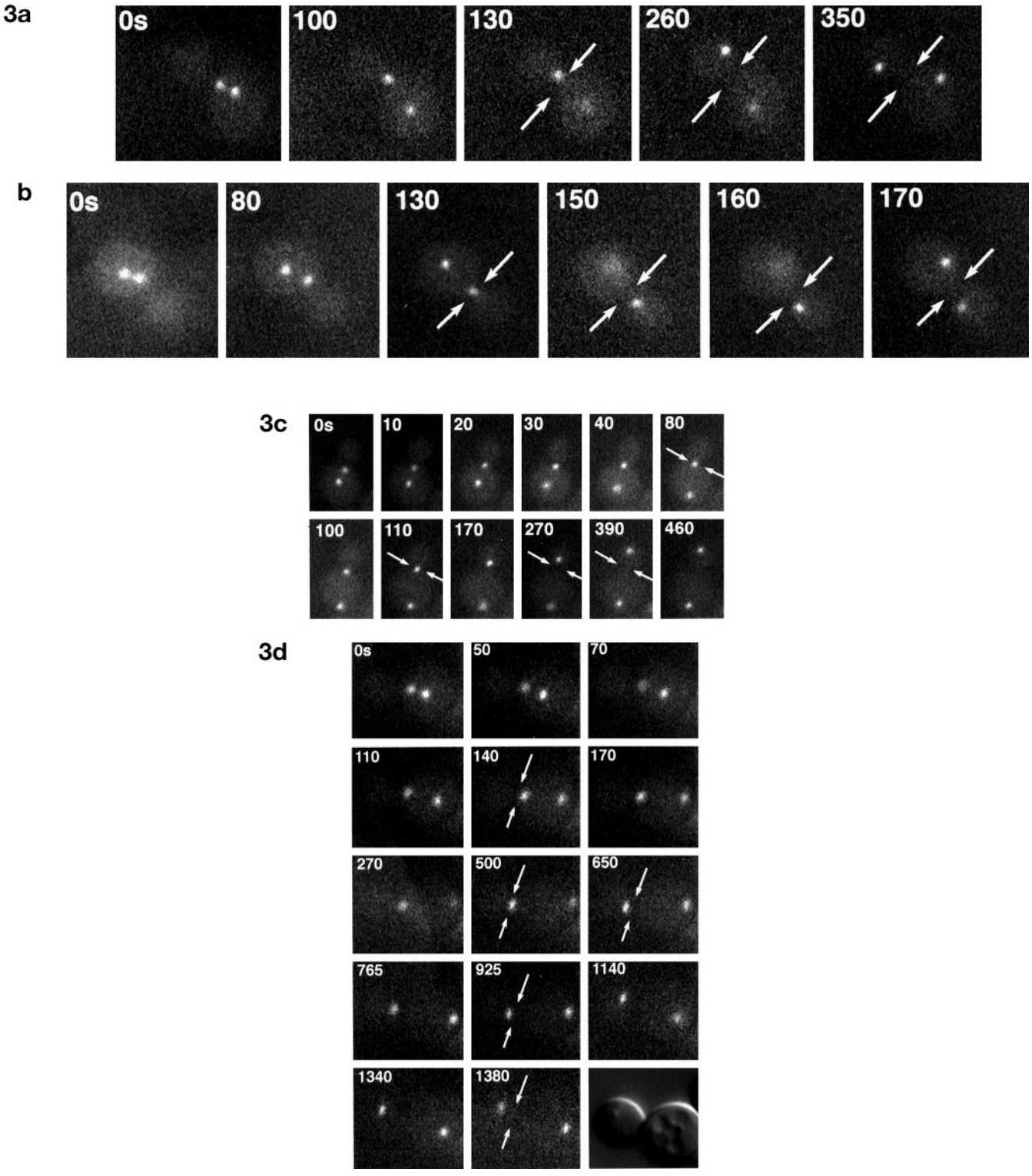

Figure 3. *In vivo* analysis of spindle movements in wild-type and *nip100*Δ cells. Wild-type JKY85 (A and B) and *nip100*Δ (JKY86) (C and D) cells expressing Nuf2-GFP were observed by time-lapse fluorescence microscopy. Live cells were observed at 10-s intervals for up to 25 min. Elapsed times are shown are in seconds. Arrows denote the position of the bud neck. (A and B) Rapid penetration of mitotic spindle through the bud neck in wild-type cells. Note that wild type cells typically translocate their mitotic spindles through the bud neck within 3 min of the advent of anaphase spindle elongation. (C) Mutant *nip100*Δ cells generally do not translocate their spindles through the bud neck. Note

away from the bud neck altogether, resulting in the type VI morphology (Figure 2A). That is, regardless of the amount of time it takes for the daughter cell's SPB to enter the bud, there is no movement of the spindle as a unit into the bud. The amount of time for which the spindle remains "stuck" in the mother cell is highly variable from cell to cell. In some cells, there is essentially no delay between the mother's SPB contacting the mother cell cortex and the daughter cell's SPB traversing the bud neck (Figure 3C). In other cells, we have observed that the delay may last from 2 to 10 min, but afterward anaphase proceeds normally (Figure 3D). Moreover, we note that the oscillations of the spindle back and forth through the bud neck observed in wild-type cells during nuclear penetration (Palmer et al., 1989; Kahana et al., 1995; Yeh et al., 1995) and absent in *dyn1*Δ cells are also absent in *nip100*Δ cells.

We have observed this "translocation-defective" phenotype in ~90% (17 of 19) of *nip100*Δ cells observed. Furthermore, a small proportion (2 of 19) of *nip100*Δ cells observed did exhibit rapid penetration of the mitotic spindle into the daughter cell. Thus, there likely exists some residual translocation activity in the absence of a functional dynactin complex. As such, we conclude that Nip100p is involved in, but not strictly required for, the movement of the elongated spindle into the bud.

To determine whether Nip100p has any function related to the actual elongation of the mitotic spindle, the rates of spindle growth in both wild-type and *nip100*Δ cells were measured. We have previously reported that wild-type cells exhibit both "fast" and "slow" phases of spindle elongation during anaphase B (Kahana *et al.*, 1995). We observed no significant difference between *NIP100* and *nip100*Δ cells in either of the two elongation phases: fast elongation occurs at 0.96 μm/min (SD, 0.11; n = 8 mitoses) in wild-type cells and 0.98 μm/s (SD, 0.20; n = 11) in *nip100*Δ cells at 25°C, whereas slow elongation occurs at 0.29 μm/min in wild-type (SD, 0.07; n = 5) and 0.26 μm/min in *nip100*Δ (SD, 0.08; n = 7) cells. We note, however, that in *nip100*Δ cells, which fail to immediately pass their spindles into the bud neck (Figure 3D), slow elongation may pause until the spindle has penetrated the bud neck and then continue at the wild-type slow elongation rate (Figure 4). Thus, any delay in the completion of anaphase in *nip100*Δ cells is due to the pause in elongation, rather than a decrease in spindle elongation rates. In conclusion, the activity of Nip100p is limited to the dynein-dependent spindle translocation step and is not involved in spindle migration to the bud neck or the actual elongation kinetics of the mitotic spindle during anaphase in wild-type cells.

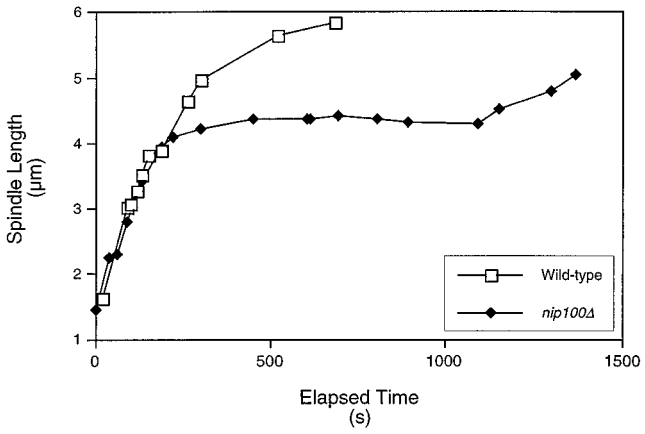

Figure 4. Kinetic analysis of spindle elongation in *nip100*Δ mutants. Kinetic diagrams of wild-type (open squares) and *nip100*Δ (filled diamonds) cells. The *nip100*Δ cell pair is shown in Figure 3D. Fast elongation for both cells (0–200 s; spindle length, <4 μm) occurs at 0.89 μm/min. Slow elongation (200–1500 s) occurs at ~0.20 μm/min in both wild-type and *nip100*Δ mutant cells. However, elongation pauses for >10 min (~300–1100 s) in the *nip100*Δ cell while the spindle is stuck within the mother cell. Rates were determined as the slope of a linear curve fit of the data points in each phase.

Genetic Interactions in nip100Δ Strains

Based on the phenotypic similarities, we sought to determine whether *nip100*Δ strains exhibited genetic interactions similar to those of strains lacking other proteins required for proper anaphase spindle partitioning. It has been reported that *dyn1*Δ; *act5*Δ and *dyn1*Δ; *jnm1*Δ strains are both viable (McMillan and Tatchell, 1994; Muhua *et al.*, 1994). Thus, we crossed a *nip100*Δ*::HIS3* strain to a *dyn1*Δ*::URA3* strain to determine whether the two disruptions exhibited "synthetic lethality." Tetrad analysis of the resulting diploid yielded 35% Ura^+, His^+ spores, indicating that the genes are not synthetically lethal. Similarly, we have observed that *nip100*Δ; *act5*Δ and *nip100*Δ; *jnm1*Δ strains are viable as well. Moreover, it has been previously shown that *nip100*Δ, *act5*Δ, and *jnm1*Δ are all synthetically lethal with null alleles of the kinesin-like protein-encoding gene *CIN8* (Geiser *et al.*, 1997). Taken together, these genetic interactions support the assertion that Nip100p, Dyn1p, Act5p, and Jnm1p all act together in a single, nonessential physiological pathway.

Figure 3 (facing page). that the spindle elongates to ~4 μm within the mother but does not translocate into the daughter. However at ~270 s after anaphase B begins, continuing spindle elongation causes the daughter spindle pole to pass through the bud neck. (D) A mother–daughter pair of *nip100*Δ cells, which fails to partition the spindle into the bud for an extended period. Note that, like the cells in C, the spindle has elongated to the mother cell cortex. However, the spindle remains in the mother for >14 min. However, at 1340 s, the spindle has elongated through the bud neck.

Biochemical Analysis of the Yeast Dynactin Complex

We sought to determine whether Nip100p exists in a large complex similar to that of its vertebrate homologue p150^{glued}. To do so, we constructed strains in which the *NIP100* open reading frame was fused to a cDNA encoding three tandem repeats of the influenza HA epitope tag. We note that the Nip100-3xHA fusion protein is functional: *cin8*Δ strains that express Nip100-3xHA in place of wild-type Nip100p grow at rates indistinguishable from *cin8*Δ*; NIP100* strains. Furthermore, we observe <2% binucleate cells in vegetatively growing strains that express Nip100-3xHA.

Cells expressing Nip100-3xHA were grown to midlogarithmic phase and lysed in the presence or absence of detergent, and the resulting extracts were spun at both low speed (13,000 rpm in a microcentrifuge) and high speed (55,000 rpm, ~100,000 × *g*). Fractions corresponding to whole cells, low-speed supernatant, low-speed pellet, high-speed supernatant, and high-speed pellet were analyzed by immunoblot using the 12CA5 monoclonal antibody against the HA tag. We observe that the Nip100-3xHA protein can be solubilized under nondenaturing conditions as long as detergent is present (Figure 5A). High-speed supernatants were further analyzed by sucrose density gradient centrifugation. Using a 7–18% sucrose gradient, we have determined that Nip100-3xHA exists in a ~15.5S complex (Figure 5B, lanes 4 and 5).

Because Nip100p, Act5p, and Jnm1p are all required for proper spindle partitioning during anaphase, we sought to determine whether we could isolate them in a stable complex in yeast. To do so, we constructed a fusion of the *NIP100* 5′ promoter sequence and entire open reading frame to a cDNA encoding four tandem repeats of the protein A IgG binding domain (hereafter referred to as "4Z") on a CEN plasmid (Grandi *et al.*, 1993). We note that the fusion protein retains the function of Nip100p; expression of the *Nip100-4Z* transgene rescues the synthetic lethality of the *nip100*Δ*; cin8*Δ double mutant and complements the anaphase spindle migration defect of *nip100*Δ strains. Cells constitutively expressing Nip100-4Z at near physiological levels were grown to midlogarithmic phase and lysed under nondenaturing conditions, and the soluble extract was incubated with a human IgG affinity matrix. After washing, bound proteins were eluted from the matrix and analyzed by SDS-PAGE and immunoblotting. As controls for binding specificity, control experiments using the 4Z polypeptide alone as well as functional fusions of 4Z to Nuf2p and the cytoplasmic dynein intermediate chain homologue Pac11p (Geiser *et al.*, 1997) were performed in parallel.

Using this method, we have determined that Nip100p exists in a stable complex with Act5p and Jnm1p in vegetatively growing yeast cells. As shown in Figure 6A, both Jnm1p and Act5p are specifically coprecipitated with Nip100-4Z (Figure 6A, lanes 1 and 2) but not with 4Z, Nuf2-4Z, or Pac11-4Z (Figure 6A lanes 3–8). In support of this, we observe that Act5p as well at the Jnm1 protein cosediment along with Nip100-3xHA in the sucrose gradient at ~15.5S (Figure 5B, top panel, lanes 4 and 5). Although essentially all of Nip100p and Act5p are detected in the 15.5S fraction, Jnm1p is found in an additional peak fraction at ~8S. This reflects that approximately half of the total Jnm1 protein exists outside the dynactin complex, possibly in a separate, smaller complex (Figure 5B, lanes 8 and 9). Furthermore. we note that the 8S but not the 15.5S portion of Jnm1p can be solubilized in detergent-free lysates.

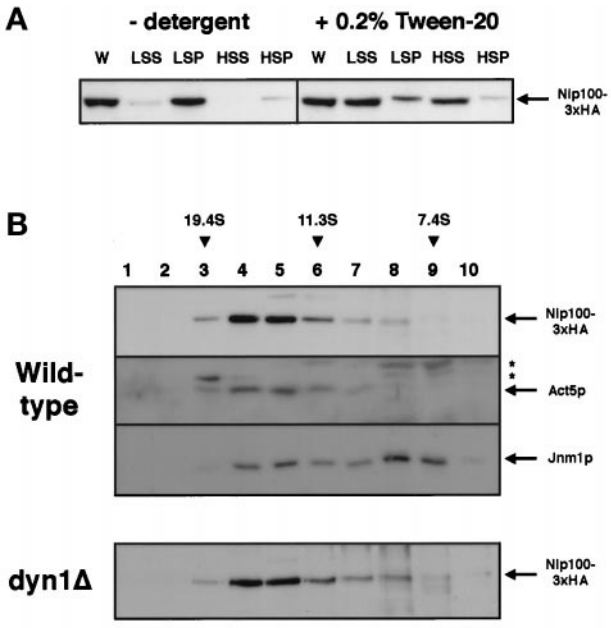

Figure 5. Biochemical characterization of the yeast dynactin complex. (A) Detergent solubility of Nip100-3xHA from whole-cell extracts. Cells expressing Nip100-3xHA were lysed in buffer with or without 0.2% Tween 20 nonionic detergent. The lysate was spun at 13,000 rpm in a microcentrifuge, and the low-speed supernatant was then spun at 55,000 rpm (~100,000 × *g*) in a tabletop ultracentrifuge. Equal fractions of the whole-cell extract (W), low-speed supernatant (LSS), low-speed pellet (LSP), high-speed supernatant (HSS), and high-speed pellet (HSP) were analyzed by immunoblotting with the 12CA5 anti-HA monoclonal antibody. (B) Sucrose density gradient centrifugation indicates that Nip100p, Act5p, and Jnm1p are all present in a 15.5S complex, which does not include cytoplasmic dynein. High-speed supernatants from wild-type or *dyn1*Δ strains expressing Nip100-3xHA were analyzed in 7–18% sucrose gradients. Ten equal fractions were collected and analyzed by SDS-PAGE and immunoblotting using antibodies against the HA tag (wild-type panel, top row; and dyn1Δ panel), Act5p (wild-type panel, second row), and Jnm1p (wild-type panel, third row). Cross-reacting bands detected by the antiAct5p antibody are denoted with an asterisk. Purified thyroglobulin (19.4S), catalase (11.3S), and yeast alcohol dehydrogenase (7.4S) were used as standards.

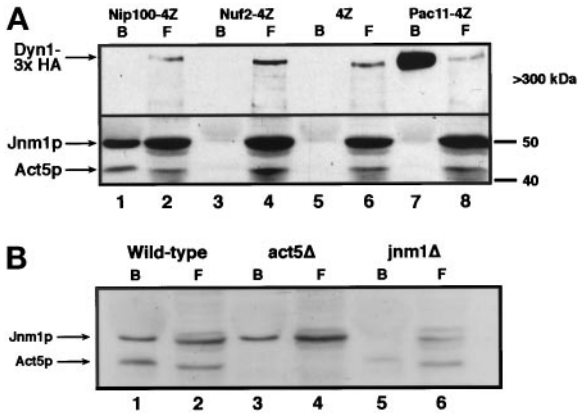

Figure 6. Direct biochemical interactions between dynactin homologues and dynein chains. Cells expressing HA-tagged Dyn1p (Dyn1-3xHA) and various protein A IgG binding site (4Z)–tagged proteins were lysed under nondenaturing conditions, and the extracts were incubated with human IgG-Sepharose beads. After washing, bound (B) and free (F) proteins were resolved by SDS-PAGE and blotted to nitrocellulose. Blots were probed with antibodies against Act5p, Jnm1p, and the HA tag. The bound fractions were concentrated 10-fold (with respect to free fractions) before electrophoresis. (A) Act5p and Jnm1p specifically coprecipitate with Nip100-4Z (lanes 1 and 2) but not with Nuf2-4Z (lanes 3 and 4), 4Z (lanes 5 and 6), or Pac11-4Z (lanes 7 and 8). Note that Act5p migrates at the expected 42 kDa, whereas Jnm1p (predicted molecular mass, 43.6 kDa) migrates at ~50 kDa. The heavy chain of cytoplasmic dynein (Dyn1-3xHA) specifically coprecipitates only with the intermediate chain (Pac11-4Z). (B) Wild-type (lanes 1 and 2), *act5*Δ (lanes 3 and 4), and *jnm1*Δ (lanes 5 and 6) cells expressing Nip100-4Z were processed as in A. Although the absence of Act5p has no effect on Jnm1p binding to Nip100-4Z, there is a 5- to 10-fold decrease in binding of Act5p to Nip100-4Z in a *jnm1*Δ strain.

In contrast, we do not observe a stable interaction between cytoplasmic dynein and the dynactin complex proteins. We expressed a functional fusion of the cytoplasmic dynein heavy chain Dyn1p to three tandem repeats of the HA epitope tag (Dyn1-3xHA) and performed the affinity precipitation experiments as above. As shown in Figure 5A, the tagged dynein heavy chain fails to appreciably coprecipitate with Nip100-4Z, Nuf2-4Z, or 4Z (Figure 5A, lanes 1–6). In contrast, Dyn1-3xHA stably interacts with the putative dynein intermediate chain Pac11-4Z (Figure 6A, lanes 7 and 8). Based on this interaction and the sequence homology, we conclude that Pac11p is indeed the yeast dynein intermediate chain.

Previous studies have demonstrated that purified cytoplasmic dynein intermediate chains can bind to p150^{glued} in vitro (Vaughan and Vallee, 1995). To test whether this phenomenon could be observed in our cell extracts, we expressed a functional fusion of Pac11p to the HA tag. In our coprecipitation experiments, we did not observe a stable interaction between Nip100-4Z and Pac11-HA. We further note that neither Act5p nor Jnm1p is coprecipitated with Pac11-4Z (Figure 6A, lanes 7 and 8). Moreover, we note that the migration of Nip100-3xHA in a sucrose gradient is identical in wild-type and *dyn1*Δ strains (Figure 5B, bottom panel, lanes 4 and 5). Thus, if there exists a physical interaction between the dynein intermediate chain and the dynactin complex, it is either transient or too unstable to detect in our assay.

Previous attempts to characterize the various interactions within the vertebrate dynactin complex have relied on ultrastructural analysis (Schafer *et al.*, 1994) or in vitro binding studies using one or more recombinant factors present in nonstoichiometric quantities (Waterman-Storer *et al.*, 1995). In contrast, because *S. cerevisiae* is genetically tractable, we could assay the arrangement of binding of Nip100p, Act5p, and Jnm1p in the yeast dynactin complex under physiological conditions by performing the affinity precipitation experiments in *act5*Δ and *jnm1*Δ strains. In one such depletion experiment, Jnm1p wholly retained its ability to bind to Nip100-4Z in strains completely lacking centractin because of a deletion of the *ACT5* gene (Figure 6B, lanes 3 and 4). In contrast, the interaction between Act5p and Nip100-4Z is dependent on the presence of Jnm1p. Although Act5p is expressed at normal levels in a *jnm1*Δ strain (Figure 6B, lanes 2 and 6), its interaction with Nip100-4Z is diminished to nearly undetectable levels (Figure 6B, lanes 5 and 6). Thus, Jnm1p mediates the interaction between Nip100p and centractin in the dynactin complex.

A Functional Fusion of Nip100 to GFP Localizes to the Spindle Poles

To localize Nip100p in living cells, we constructed a fusion of the full-length *NIP100* gene (with its promoter) to the GFP cDNA. Expression of the fusion gene from a CEN plasmid rescues the inviability of *nip100*Δ*; cin8*Δ strains, but no fluorescence is observed in living cells. However, when Nip100-GFP is constitutively expressed from a multicopy (2μ) plasmid, one or two perinuclear dots were observed in ~10% of cells in culture. To confirm that the dots coincided with the spindle poles, we performed double-label indirect immunofluorescence using antibodies against α-tubulin and GFP. As illustrated in Figure 7A, Nip100-GFP colocalizes with the single SPB in G_1 cells and at the spindle poles of dividing cells throughout mitosis. This is consistent with the previously described localization of the mammalian p50 and p150^{glued} dynactin complex proteins and the *Drosophila* Glued protein to the centrosomes of mitotic cells (Gill *et al.*, 1991; Paschal and Vallee, 1993; Waterman-Storer and Holzbaur, 1996) as well as the spindle pole and microtubule association previously described for Jnm1p (McMillan and Tatchell, 1994). However, whereas Jnm1p was usually found associated with a single SPB, Nip100-GFP is found at both ends of the

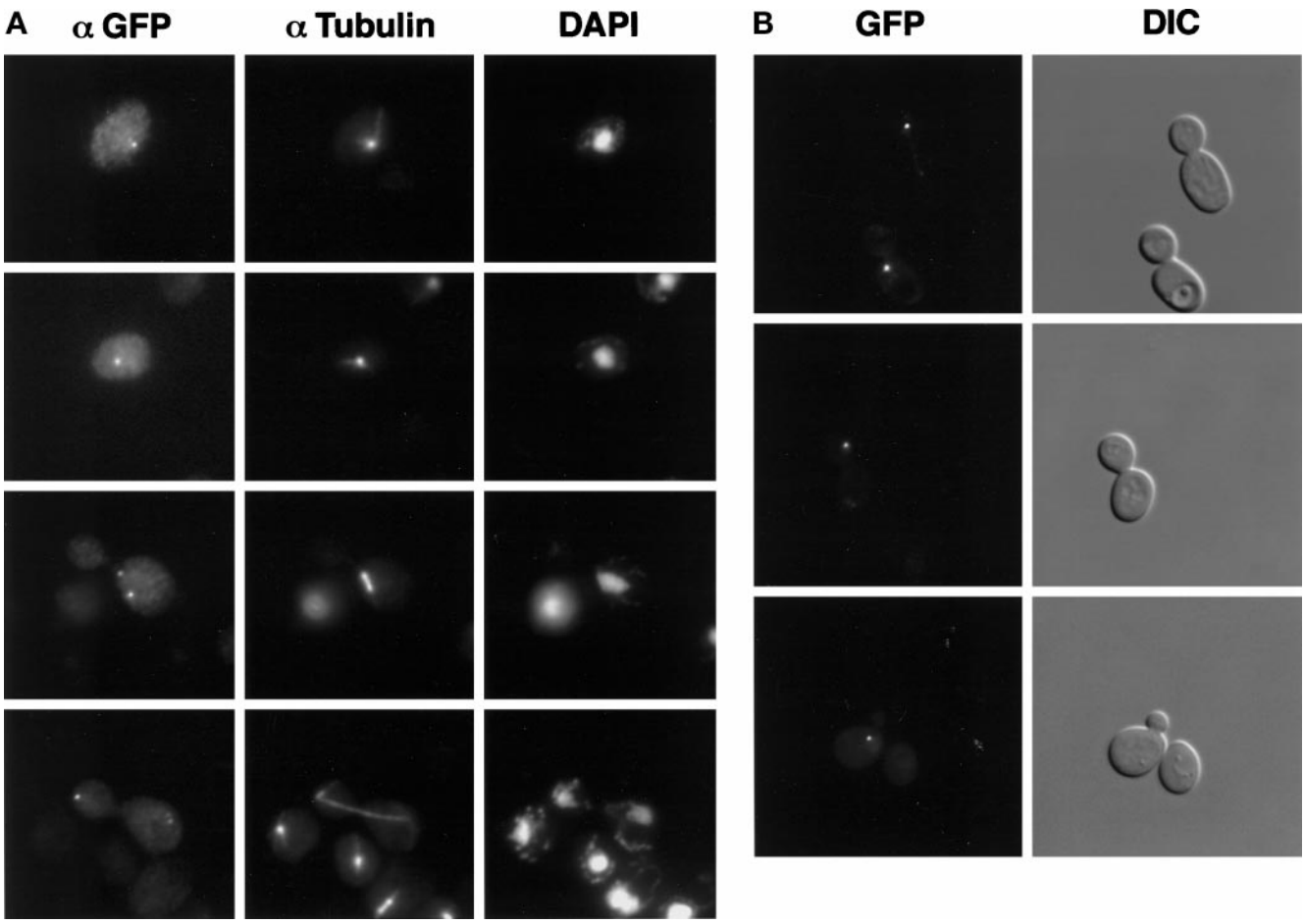

Figure 7. Nip100 localizes to the spindle poles of vegetatively growing cells throughout the cell cycle. (A) Strain JKY77 (*nip100*Δ*::HIS3*) overexpressing Nip100-GFP from a 2μ plasmid was grown to midlogarithmic phase and processed for immunofluorescence. Nip100-GFP was visualized with a polyclonal antibody against GFP followed by FITC-conjugated secondary antibodies. Microtubules were visualized with a monoclonal antibody against α-tubulin followed by Texas Red-conjugated secondary antibodies. Chromatin was visualized with DAPI. (B) Pulse–chase expression of Nip100-GFP using the *GAL1–10* promoter. Nip100-GFP was expressed for 30 min using 2% galactose and then repressed for 3 h using 2% glucose as the sole carbon source. In 58% of large-budded cells, Nip100-GFP is predominantly localized to the SPB, which is in the daughter cell (top two panels). In small and medium (preanaphase B) cells, Nip100-GFP is typically associated with a single SPB at the bud neck (bottom panel).

mitotic spindle in dividing cells. Although the Nip100-GFP protein is functional, we cannot discount the possibility that this "extra" localization may be a consequence of overexpressing the fusion protein.

To address this possibility, we performed a pulse–chase experiment by expressing Nip100-GFP from the inducible *GAL1–10* promoter (Yocum et al., 1984). Nip100-GFP was expressed transiently by addition of 2% galactose to the medium for 30 min followed by growth for 3 h in medium containing 2% glucose (which strongly inhibits the *GAL1–10* promoter). Under these conditions, we observe a distribution of Nip100-GFP that is more similar to that reported for Jnm1p (Figure 7B); typically, we observe Nip100-GFP associated with a single pole in unbudded and small-budded (G_1–S) cells (Figure 7B, bottom row). In large (G_2–M) budded cells, we observe Nip100-GFP preferentially at the daughter cell's spindle pole (58% in daughter, 25% in mother, and 17% on both spindle poles). In contrast, we do not observe preferential localization of Nuf2-GFP to a single SPB under similar pulse–chase expression conditions (Kahana et al., 1995). Furthermore, we do not observe association with astral microtubules, as has been reported for fragments of dynein fused to GFP and expressed under similar conditions (Shaw et al., 1997).

DISCUSSION

In this study, we have shown by phenotypic, biochemical, and genetic criteria that the *NIP100* gene encodes the yeast homologue of the vertebrate dynactin pro-

tein p150^{glued}. Strains lacking Nip100p have anaphase spindle misorientation defects indistinguishable from those previously reported for *dyn1*Δ, *act5*Δ, and *jnm1*Δ strains because of their inability to translocate elongated spindles into the daughter cell during anaphase. Furthermore, Nip100p exists in a stable complex with both centractin and Jnm1p but not with the heavy or intermediate chains of cytoplasmic dynein. Moreover, *nip100*Δ strains exhibit genetic interactions identical to those of *act5*Δ and *jnm1*Δ strains. Finally, we have observed that Nip100-GFP localizes the spindle poles throughout the cell cycle. These results are discussed in terms of the potential physiological role of the dynactin complex in anaphase spindle partitioning.

A Physiological Role for Dynein and Dynactin

Although the biochemical activities of cytoplasmic dynein and dynactin have been well characterized in vitro, the physiological role of these factors is not yet clear. Previous studies have suggested a requirement for dynein in spindle assembly in vertebrate cells (Vaisberg *et al.*, 1993; Gaglio *et al.*, 1995, 1996; Heald *et al.*, 1996; Merdes *et al.*, 1996); however, spindle formation and elongation during anaphase are not defective in yeast strains lacking dynein. We note that dynein and dynactin genes are essential in yeast strains lacking the kinesin-like protein Cin8p, which is involved in spindle assembly and elongation (Hoyt *et al.*, 1992; Saunders *et al.*, 1995). Similarly, it has been shown that both dynein and the kinesin-like protein Eg5 are required for spindle assembly in mammalian cells (Gaglio, *et al.*, 1996). However, the activity of kinesin in yeast may itself be sufficient to elicit spindle formation in the absence of dynein and dynactin.

Studies using *Drosophila* have shown that cytoplasmic dynein and Glued are required for proper development of the fly. Dominant hemizygous mutations in the *Glued* gene (*Gl*^{l}) and heteroallelic mutations in the *Dhc64C* (dynein heavy chain) gene lead to defects in eye development (Meyerowitz and Kankel, 1978; Harte and Kankel, 1983; Garen *et al.*, 1984; Swaroop *et al.*, 1985, 1987; McGrail *et al.*, 1995). Furthermore, it has been shown that flies homozygous for the *Gl*^{l} mutation or null alleles of *Glued* are inviable (Garen and Kankel, 1983; Swaroop *et al.*, 1986). Recently, a more precise determination of the role of dynein during ontogeny has been determined; early in oogenesis, dynein is required for proper spindle orientation in dividing cysts (McGrail and Hays, 1997). This finding is compatible with the finding that yeast strains bearing mutations in dynein or dynactin genes have spindle migration defects during mitosis.

Cytogenetic studies using *S. cerevisiae* strains deficient for *ACT5*, *JNM1*, *NIP100*, and *DYN1* have clearly shown that dynein and dynactin are involved in, but not required for, spindle partitioning during anaphase B. Our finding that Nip100p is involved in the translocation of the elongated mitotic spindle into the bud is consistent with a previous study implicating cytoplasmic dynein in nuclear migration (Yeh *et al.*, 1995). However, our finding that a small percentage (10.5%) of *nip100*Δ cells exhibit "normal" spindle translocation kinetics suggests that either dynein has residual activity in the absence of dynactin, or there exists some independent yet redundant activity involved in translocation which cooperates with dynein and dynactin.

The Roles of Dynein, Dynactin, and Kinesin in Anaphase Spindle Partitioning

The dynamic behavior of strains lacking Nip100p is virtually identical to that of strains lacking the heavy chain of dynein. Yeh, *et al.* (1995) have shown that like *nip100*Δ *dyn1*Δ strains are generally defective in their ability to pass elongating spindles through the bud neck. In contrast, it has recently been shown that strains lacking the kinesin-like protein Kip3p have a distinct type of dynamic defect in anaphase spindle partitioning. Like strains lacking dynein or dynactin complex proteins, *kip3*Δ strains accumulate binucleate and anucleate cells because of failure to pass the mitotic spindle into the bud. However, this phenotype is due to a defect in an earlier step of mitosis: the movement of the nucleus to the bud neck prior to anaphase B. Furthermore, *kip3*Δ; *dyn1*Δ strains are poorly viable, suggesting that the essential function of partitioning of the mitotic spindle between mother and daughter is effected by two sequential but redundant activities (Cottingham and Hoyt, 1997; DeZwaan *et al.*, 1997). Because the role of dynactin was defined in an in vitro assay, and the static phenotypes of *nip100*Δ, *act5*Δ, *jnm1*Δ, and *kip3*Δ strains are similar, it was possible that dynactin was required for the function of more than one motor protein during anaphase. However, based on the behavior of *nip100*Δ cells in our in vivo assay, it is clear that dynactin acts with dynein in the translocation step but is not involved in the Kip3-dependent nuclear migration step.

How do cytoplasmic dynein and dynactin together effect spindle translocation during anaphase? Previous models have suggested that dynein may translocate the mitotic spindle into the bud by pulling the minus ends of the astral microtubules toward the daughter cell cortex (Eshel *et al.*, 1993). Furthermore, it has recently been demonstrated that interactions between the astral microtubules and the cell cortex are required for spindle translocation (Carminati and Stearns, 1997). As such, it was theorized that dynactin could serve to tether cytoplasmic dynein at the cell cortex (McMillan and Tatchell, 1994; Schroer, 1994). However, Nip100-GFP is never observed at the cell cortex even when overexpressed: In all phases of the cell cycle, Nip100-GFP is found at the spindle poles. This

localization would be more consistent with dynein indirectly providing a plus-end–directed force, which pulls the spindle into the bud via the daughter's astral microtubules. For instance, dynein and dynactin may promote spindle translocation by depolymerizing daughter astral microtubules at the spindle poles in a manner similar to that previously demonstrated for vertebrate kinesin (Coue *et al.*, 1991; Lombillo *et al.*, 1995a,b). We note that in strains lacking dynein or the yeast dynactin proteins, binucleate cells with abnormally long astral microtubules can be observed (Clark and Meyer, 1994; McMillan and Tatchell, 1994; Geiser et al., 1997; this study). Thus, the failure to translocate spindles may be simply due to steric hindrance by abnormally stable astral microtubules in the daughter cell. In support of this theory is the finding that the synthetic lethality of a *dyn1*Δ*; kip3*Δ double mutant can be rescued by the additional disruption of the *KIP2* gene, whose product is involved in stabilization of astral microtubules (Cottingham and Hoyt, 1997; Huyett et al., 1998).

Interactions within the Dynactin Complex

The novel finding that Jnm1p is coprecipitated with the centractin and p150^{glued} homologues indicates that it is a member of the yeast analog of the dynactin complex. Like vertebrate p50, Jnm1p is predicted to comprise three large coiled-coil domains (McMillan and Tatchell, 1994; Echeverri *et al.*, 1996). Taken together with the phenotypic similarity between *jnm1*Δ, *nip100*Δ, and *act5*Δ strains, these results suggest that, despite extremely weak sequence homology, Jnm1p is the yeast homologue of dynactin protein p50.

Because neither *ACT5* nor *JNM1* is an essential gene, we have been able to use a "genetic depletion" technique to partially characterize the interactions between dynactin complex proteins. Our finding that Jnm1p is required for the full binding of Act5p to Nip100p suggests that centractin binds to the dynactin complex in a cooperative manner. It has previously been shown that purified p150^{glued} binds to purified centractin in vitro (Waterman-Storer *et al.*, 1995). Our result that binding of Nip100-4Z to Act5p is greatly diminished but not completely ablated in a *jnm1*Δ strain is consistent with the in vitro data. However, the fact that significantly less Act5p is coprecipitated with Nip100-4Z in *jnm1*Δ versus wild-type extracts suggests that Act5p cooperatively binds to Jnm1p (or a factor bound to it) and Nip100p, or that Jnm1p may form a "scaffold" for an Act5 filament. However, our finding that Act5p is not required for Jnm1 binding to Nip100-4Z indicates that any structure formed by Jnm1p can assemble and bind to the rest of the complex independently of a filamentous centractin structure. Moreover, our finding that a portion of the Jnm1 protein exists in an ~8S state raises the possibility that it can form a multimeric structure independently of the rest of the dynactin complex.

We have observed that cytoplasmic dynein does not stably interact with dynactin complex proteins in our affinity chromatography assay. This finding is consistent with the previous observation that cytoplasmic dynein is not coimmunoprecipitated with p50 from bovine brain extracts (Paschal *et al.*, 1993). However, several groups have demonstrated an in vitro interaction between the intermediate chain of dynein and p150^{glued} (Karki and Holzbaur, 1995; Vaughan and Vallee, 1995). A previous explanation for this discrepancy is that antibodies used to immunoprecipitate dynein and p50 blocked the interaction between the two proteins (Karki and Holzbaur, 1995). However, in our experiments, a C-terminal affinity tag was used to purify the full-length p150^{glued} and dynein intermediate chain homologues. Because the inclusion of the 4Z tag at the C terminus did not adversely affect the in vivo function of either Nip100p or Pac11p, it is unlikely that binding of IgG to the tagged proteins interrupted such an interaction. Moreover, we note that the migration of the complex in a sucrose density gradient is unaffected by the "genetic depletion" of the dynein heavy chain. Finally, we note that, in the original purification of dynactin from chick brain extracts, dynein, but not individual dynactin components, could be separated from the complex by ion-exchange chromatography (Schroer *et al.*, 1988).

How does dynactin regulate cytoplasmic dynein's function if the two do not form a stable complex? Based on the requirement for dynactin in dynein-mediated vesicle motility and the ability of p150^{glued} to bind to the dynein intermediate chain in vitro, we suggest that there exists an interaction between dynein and dynactin that is transient and possibly inhibited by additional factors. In contrast to the in vitro binding studies, our coprecipitation assay does not rely on the presence of a large excess of one or more of the factors and is done in the presence of other (possibly inhibitory) cellular factors. Thus, our inability to detect a complex possibly reflects an in vivo interaction that is too transient to coprecipitate. For instance, if dynactin has an enzymatic role in the activation of dynein, then a stable interaction would not be expected.

In conclusion, the fact that yeast dynactin proteins behave analogously to their vertebrate and insect counterparts indicates that *S. cerevisiae* is a useful model system for the study of dynein function. Consequently, the use of the genetically tractable yeast system affords us the ability to study the physiological roles of dynein and dynactin in living cells. Furthermore, the finding that *dyn1*Δ, *act5*Δ, *jnm1*Δ, and *nip100*Δ strains require *CIN8* for viability suggests that other factors that exhibit pairwise lethality with *cin8*Δ may be involved in dynein and dynactin function

(Geiser *et al.*, 1997). Using the combination of genetic, cytological, and biochemical techniques described herein, we should be able to further characterize the roles and behavior of these factors during the cell cycle.

ACKNOWLEDGMENTS

We thank Sean Clark, David Meyer, Mashid Company, John McMillan, and Kelly Tatchell for unpublished antibodies was well as Paul Ferrigno, Anita Corbett, Janet Carminati, Becket Feierbach, Tim Stearns, Erika Holzbaur, Frank Cottingham, Todd DeZwaan, David Roof, Kerry Bloom, and Trina Schroer for helpful discussions and results before publication. We are also grateful for technical assistance from Scott Schuyler, Lieu Anh Nguyen, Barry Alpert, Paul Milman, and T.R. Magliozzi. This work was supported by a Claudia Adams Barr investigator award and a grant from the National Institutes of Health to P.A.S. as well as grants from the March of Dimes and the National Institutes of Health to M.A.H. J.A.K. is supported by a predoctoral training grant from the National Institutes of Health. G.S. was supported by a postdoctoral grant from the Deutsche Forschungsgemeinschaft. J.R.G. is supported by a postdoctoral fellowship from the Cancer Research Fund of the Damon Runyon–Walter Winchell Foundation.

REFERENCES

Altschul, S.F., Gish, W., Miller, W., Myers, E.W., and Lipman, D.J. (1990). Basic local alignment search tool. J. Mol. Biol. *215*, 403–410.

Baudin, A., Ozier-Kalogeropoulos, O., Denouel, A., Lacroute, F., and Cullin, C. (1993). A simple and efficient method for direct gene deletion in Saccharomyces cerevisiae. Nucleic Acids Res. *21*, 3329–3330.

Carminati, J.L., and Stearns, T. (1997). Microtubules orient the mitotic spindle in yeast through dynein- dependent interactions with the cell cortex. J. Cell Biol. *138*, 629–641.

Clark, S.W., and Meyer, D.I. (1994). ACT3: a putative centractin homologue in *S. cerevisiae* is required for proper orientation of the mitotic spindle. J. Cell Biol. *127*, 129–138.

Cottingham, F.C., and Hoyt, M.A. (1997). Mitotic spindle positioning in *Saccharomyces cerevisiae* is accomplished by antagonistically acting microtubule motor proteins. J. Cell Biol. *138*, 1041–1053.

Coue, M., Lombillo, V.A., and McIntosh, J.R. (1991). Microtubule depolymerization promotes particle and chromosome movement in vitro. J. Cell Biol. *112*, 1165–1175.

DeZwaan, T.M., Ellingson, E., Pellman, D., and Roof, D.R. (1997). Kinesin-related KIP3 of *Saccharomyces cerevisiae* is required for a distinct step in nuclear migration. J. Cell Biol. *138*, 1023–1040.

Echeverri, C.J., Paschal, B.M., Vaughan, K.T., and Vallee, R.B. (1996). Molecular characterization of the 50-kD subunit of dynactin reveals function for the complex in chromosome alignment and spindle organization during mitosis. J. Cell Biol. *132*, 617–633.

Eshel, D., Urrestarazu, L.A., Vissers, S., Jauniaux, J.C., van Vliet-Reedijk, J.C., Planta, R.J., and Gibbons, I.R. (1993). Cytoplasmic dynein is required for normal nuclear segregation in yeast. Proc. Natl. Acad. Sci. USA *90*, 11172–11176.

Gaglio, T., Saredi, A., Bingham, J.B., Hasbani, M.J., Gill, S.R., Schroer, T.A., and Compton, D.A. (1996). Opposing motor activities are required for the organization of the mammalian mitotic spindle pole. J. Cell Biol. *135*, 399–414.

Gaglio, T., Saredi, A., and Compton, D.A. (1995). NuMA is required for the organization of microtubules into aster-like mitotic arrays. J. Cell Biol. *131*, 693–708.

Garen, A., Miller, B.R., and Paco-Larson, M.L. (1984). Mutations affecting functions of the *Drosophila* gene glued. Genetics *107*, 645–655.

Garen, S.H., and Kankel, D.R. (1983). Golgi and genetic mosaic analyses of visual system mutants in *Drosophila melanogaster*. Dev. Biol. *96*, 445–466.

Geiser, J.R., Schott, E.J., Kingsbury, T.J., Cole, N.B., Totis, L.J., Bhattacharyya, G., He, L., and Hoyt, M.A. (1997). *Saccharomyces cerevisiae* genes required in the absence of the CIN8-encoded spindle motor act in functionally diverse mitotic pathways. Mol. Biol. Cell *8*, 1035–1050.

Gietz, R.D., and Schiestl, R.H. (1991). Applications of high efficiency lithium acetate transformation of intact yeast cells using single-stranded nucleic acids as carrier. Yeast *7*, 253–263.

Gill, S.R., Schroer, T.A., Szilak, I., Steuer, E.R., Sheetz, M.P., and Cleveland, D.W. (1991). Dynactin, a conserved, ubiquitously expressed component of an activator of vesicle motility mediated by cytoplasmic dynein. J. Cell Biol. *115*, 1639–1650.

Grandi, P., Doye, V., and Hurt, E.C. (1993). Purification of NSP1 reveals complex formation with "GLFG" nucleoporins and a novel nuclear pore protein NIC96. EMBO J, *12*, 3061–3071.

Harte, P.J., and Kankel, D.R. (1983). Analysis of visual system development in *Drosophila melanogaster*: mutations at the Glued locus. Dev. Biol. *99*, 88–102.

Heald, R., Tournebize, R., Blank, T., Sandaltzopoulos, R., Becker, P., Hyman, A., and Karsenti, E. (1996). Self-organization of microtubules into bipolar spindles around artificial chromosomes in *Xenopus* egg extracts (see comments). Nature, *382*, 420–425.

Holzbaur, E.L., Hammarback, J.A., Paschal, B.M., Kravit, N.G., Pfister, K.K., and Vallee, R.B. (1991). Homology of a 150K cytoplasmic dynein-associated polypeptide with the *Drosophila* gene Glued. Nature *351*, 579–583 (erratum *360*, 695).

Hoyt, M.A., He, L., Loo, K.K., and Saunders, W.S. (1992). Two *Saccharomyces cerevisiae* kinesin-related gene products required for mitotic spindle assembly. J. Cell Biol. *118*, 109–120.

Huyett, A., Kahana, J., Silver, P., Zeng, X., and Saunders, W. (1998). The Kar3p and Kip2p motors function antagonistically at the spindle poles to influence cytoplasmic microtubule numbers. J. Cell Sci. *111*, 295–301.

Kahana, J.A., Schnapp, B.J., and Silver, P.A. (1995). Kinetics of spindle pole body separation in budding yeast. Proc. Natl. Acad. Sci. USA *92*, 9707–9711.

Kahana, J.A., and Silver, P.A. (1996). Use of the *A. victoria* green fluorescent protein to study protein dynamics in vivo. In: Current Protocols in Molecular Biology, ed. F.M. Ausubel, R. Brent, R.E. Kingston, D.E. Moore, J.G. Seidman, J.A. Smith, and K. Struhl, New York: John Wiley & Sons, 9.6.13–9.6.19.

Karki, S., and Holzbaur, E.L. (1995). Affinity chromatography demonstrates a direct binding between cytoplasmic dynein and the dynactin complex. J. Biol. Chem. *270*, 28806–28811.

Lees-Miller, J.P., Helfman, D.M., and Schroer, T.A. (1992). A vertebrate actin-related protein is a component of a multisubunit complex involved in microtubule-based vesicle motility (see comments). Nature *359*, 244–246.

Li, Y.Y., Yeh, E., Hays, T., and Bloom, K. (1993). Disruption of mitotic spindle orientation in a yeast dynein mutant. Proc. Natl. Acad. Sci. USA, *90*, 10096–10100.

Lombillo, V.A., Nislow, C., Yen, T.J., Gelfand, V.I., and McIntosh, J.R. (1995a). Antibodies to the kinesin motor domain and CENP-E inhibit microtubule depolymerization-dependent motion of chromosomes in vitro (see comments). J. Cell Biol. *128*, 107–115.

Lombillo, V.A., Stewart, R.J., and McIntosh, J.R. (1995b). Minus-end-directed motion of kinesin-coated microspheres driven by microtubule depolymerization. Nature *373*, 161–164.

Lupas, A., Van Dyke, M., and Stock, J. (1991). Predicting coiled coils from protein sequences. Science, *252*, 1162–1164.

McGrail, M., Gepner, J., Silvanovich, A., Ludmann, S., Serr, M., and Hays, T.S. (1995). Regulation of cytoplasmic dynein function in vivo by the *Drosophila* Glued complex. J. Cell Biol. *131*, 411–425.

McGrail, M., and Hays, T.S. (1997). The microtubule motor cytoplasmic dynein is required for spindle orientation during germline cell divisions and oocyte differentiation in *Drosophila*. Development *124*, 2409–2419.

McMillan, J.N., and Tatchell, K. (1994). The JNM1 gene in the yeast *Saccharomyces cerevisiae* is required for nuclear migration and spindle orientation during the mitotic cell cycle. J. Cell Biol., *125*, 143–158.

Merdes, A., Ramyar, K., Vechio, J.D., and Cleveland, D.W. (1996). A complex of NuMA and cytoplasmic dynein is essential for mitotic spindle assembly. Cell *87*, 447–458.

Meyerowitz, E., and Kankel, D.R. (1978). A genetic analysis of visual system development in *Drosophila melanogaster*. Dev. Biol. *62*, 112–142.

Muhua, L., Karpova, T.S., and Cooper, J.A. (1994). A yeast actin-related protein homologous to that in vertebrate dynactin complex is important for spindle orientation and nuclear migration. Cell *78*, 669–679.

Osborne, M.A., Schlenstedt, G., Jinks, T., and Silver, P.A. (1994). Nuf2, a spindle pole body-associated protein required for nuclear division in yeast. J. Cell Biol. *125*, 853–866.

Palmer, R.E., Koval, M., and Koshland, D. (1989). The dynamics of chromosome movement in the budding yeast *Saccharomyces cerevisiae*. J. Cell Biol., *109*, 3355–3366.

Palmer, R.E., Sullivan, D.S., Huffaker, T., and Koshland, D. (1992). Role of astral microtubules and actin in spindle orientation and migration in the budding yeast, *Saccharomyces cerevisiae*. J. Cell Biol., *119*, 583–593.

Paschal, B.M., Holzbaur, E.L., Pfister, K.K., Clark, S., Meyer, D.I., and Vallee, R.B. (1993). Characterization of a 50-kDa polypeptide in cytoplasmic dynein preparations reveals a complex with $p150^{glued}$ and a novel actin. J. Biol. Chem. *268*, 15318–15323.

Paschal, B.M., and Vallee, R.B. (1993). Microtubule and axoneme gliding assays for force production by microtubule motor proteins. Methods Cell Biol. *39*, 65–74.

Paschal, B.M., and Vallee, R.B. (1987). Retrograde transport by the microtubule-associated protein MAP 1C. Nature *330*, 181–183.

Pierre, P., Pepperkok, R., and Kreis, T.E. (1994). Molecular characterization of two functional domains of CLIP-170 in vivo. J. Cell Sci. *107*, 1909–1920.

Pierre, P., Scheel, J., Rickard, J.E., and Kreis, T.E. (1992). CLIP-170 links endocytic vesicles to microtubules. Cell *70*, 887–900.

Pringle, J.R., Adams, A.E.M., Drubin, D.G., and Haarer, B.K. (1991). Immunofluorescence methods for yeast. Methods Enzymol. *194*, 565–608.

Roeder, G.S., and Fink, G.R. (1980). DNA rearrangements associated with a transposable element in yeast. Cell *21*, 239–249.

Sambrook, J., Fritsch, E.F., and Maniatis, T. (1989). Molecular Cloning: A Laboratory Manual, Cold Spring Harbor, NY: Cold Spring Harbor Laboratory.

Saunders, W.S., Koshland, D., Eshel, D., Gibbons, I.R., and Hoyt, M.A. (1995). *Saccharomyces cerevisiae* kinesin- and dynein-related proteins required for anaphase chromosome segregation. J. Cell Biol. *128*, 617–624.

Schafer, D.A., Gill, S.R., Cooper, J.A., Heuser, J.E., and Schroer, T.A. (1994). Ultrastructural analysis of the dynactin complex: an actin-related protein is a component of a filament that resembles F-actin. J. Cell Biol. *126*, 403–412.

Schneider, B.L., Seufert, W., Steiner, B., Yang, Q.H., and Futcher, A.B. (1995). Use of polymerase chain reaction epitope tagging for protein tagging in *Saccharomyces cerevisiae*. Yeast *11*, 1265–1274.

Schroer, T.A. (1994). New insights into the interaction of cytoplasmic dynein with the actin-related protein, Arp1. J. Cell Biol. *127*, 1–4.

Schroer, T.A., Schnapp, B.J., Reese, T.S., and Sheetz, M.P. (1988). The role of kinesin and other soluble factors in organelle movement along microtubules. J. Cell Biol. *107*, 1785–1792.

Schroer, T.A., and Sheetz, M.P. (1991). Two activators of microtubule-based vesicle transport. J. Cell Biol. *115*, 1309–1318.

Shaw, S.L., Yeh, E., Maddox, P., Salmon, E.D., and Bloom, K. (1997). Astral microtubule dynamics in yeast: a microtubule-based searching mechanism for spindle orientation and nuclear migration into the bud. J. Cell Biol. *139*, 985–994.

Sherman, F., Hicks, J.B., and Fink, G.R. (1986). Methods in Yeast Genetics, Cold Spring Harbor, NY: Cold Spring Harbor Laboratory.

Sikorski, R.S., and Hieter, P. (1989). A system of shuttle vectors and yeast host strains designed for efficient manipulation of DNA in *Saccharomyces cerevisiae*. Genetics, *122*, 19–27.

Swaroop, A., Paco-Larson, M.L., and Garen, A. (1985). Molecular genetics of a transposon-induced dominant mutation in the *Drosophila* locus Glued. Proc. Natl. Acad. Sci. USA *82*, 1751–1755.

Swaroop, A., Sun, J.W., Paco-Larson, M.L., and Garen, A. (1986). Molecular organization and expression of the genetic locus glued in *Drosophila melanogaster*. Mol. Cell. Biol. *6*, 833–841.

Swaroop, A., Swaroop, M., and Garen, A. (1987). Sequence analysis of the complete cDNA and encoded polypeptide for the Glued gene of *Drosophila* melanogaster. Proc. Natl. Acad. Sci. USA *84*, 6501–6505.

Vaisberg, E.A., Koonce, M.P., and McIntosh, J.R. (1993). Cytoplasmic dynein plays a role in mammalian mitotic spindle formation. J. Cell Biol. *123*, 849–858.

Vaughan, K.T., and Vallee, R.B. (1995). Cytoplasmic dynein binds dynactin through a direct interaction between the intermediate chains and p150Glued. J. Cell Biol. *131*, 1507–1516.

Waterman-Storer, C.M., and Holzbaur, E.L. (1996). The product of the *Drosophila* gene, Glued, is the functional homologue of the p150Glued component of the vertebrate dynactin complex. J. Biol. Chem. *271*, 1153–1159.

Waterman-Storer, C.M., Karki, S., and Holzbaur, E.L. (1995). The p150Glued component of the dynactin complex binds to both microtubules and the actin-related protein centractin (Arp-1). Proc. Natl. Acad. Sci. USA *92*, 1634–1638.

Winston, F., Dollard, C., and Ricupero-Hovasse, S.L. (1995). Construction of a set of convenient *Saccharomyces cerevisiae* strains that are isogenic to S288C. Yeast *11*, 53–55.

Yeh, E., Skibbens, R.V., Cheng, J.W., Salmon, E.D., and Bloom, K. (1995). Spindle dynamics and cell cycle regulation of dynein in the budding yeast, *Saccharomyces cerevisiae*. J. Cell Biol. *130*, 687–700.

Yocum, R.R., Hanley, S., West, R., Jr., and Ptashne, M. (1984). Use of lacZ fusions to delimit regulatory elements of the inducible divergent GAL1-GAL10 promoter in *Saccharomyces cerevisiae*. Mol. Cell. Biol. *4*, 1985–1998.